The Application of Multigrid Finite Volume to Ligand-Receptor Interaction in Capillary

Wensheng Shen*
Laboratory for High Performance Scientific Computing and Computer Simulation,
Department of Computer Science, University of Kentucky,
Lexington, KY 40506–0046, USA

January 8, 2007

Abstract

This paper describes a new application of multigrid finite volume method to protein transport and protein-protein interaction in capillary. The flow in capillary is assumed laminar and simulated by incompressible Navier-Stokes equations. Proteins are considered as macromolecules and their transport in capillary is modeled by a convection-diffusion transport equation. Proteins in flow interact with those on capillary surface by a series of biochemical reactions. Finite volume method is preferred in discretizing differential equations and multigrid V-cycle algorithm is used to solve the elliptical equation for fast solution, which allows for non-uniform grid spacing and any level of grids. Three iterative methods, Stone's SIP, BiCGSTAB and GMRES are used to solve the linear system, and their performance is compared.

Key words: Multigrid, Finite volume, Navier-Stokes equation, Protein transport, Incompressible flow, Iterative method.

1 Introduction

Proteins are biological macromolecules that exist in all living organisms and are of vital importance to cell activities. Many cells activate or are activated through cell signaling and signal transduction. In the process, some proteins transmit a signal from the host cell and others work as receptors binding to the signaling molecule. This process is essential for normal physiology as well as disease healing. Typical examples of the process include, but are not limited to, the binding of antibodies to antigens, the transport of oxygen through haemoglobin. We model this process as blood flow in capillary by incompressible Navier-Stokes equation, protein transport by convection-diffusion, and local bioreaction on capillary surface.

Developing efficient solvers for nonlinear system of equations arising from fluid flow and mass transfer problems is still of big interest. When nonlinear partial differential equations are

*E-mail: wensheng@csr.uky.edu.

discretized in a particular spatial mesh, the result is a set of ordinary differential equations, with time as the independent variable,

$$\frac{df(\vec{u})}{dt} + \Phi(\vec{u}) = 0, \qquad \vec{u} \in R^n \tag{1}$$

where n is the number of control volumes in finite volume method. The temporary terms may be further discretized using either an explicit or an implicit scheme. In an explicit method, a large number of independent equations, one for each control volume, have to be solved. In case of an implicit discretization, we have to solve a large set of simultaneous equations,

$$F(\vec{u}) = \frac{f(\vec{u}) - f(\vec{u})^o}{\Delta t} + \Phi(\vec{u}) = 0 \tag{2}$$

where $f(\vec{u})^o$ is the value at the previous time step. If the number of components of $\vec{u}$ is m, the number of independent variables is mn. Such large sets of nonlinear equations are generally solved by a variant of Newton's method, where a sequence of linear systems are solved. The great advantage of the Newton iteration is its quadratic convergence. However, Newton iteration converges only if the initial guess is close to the solution. Instead, in this paper, the method of Picard iteration is applied, in which the nonlinear convective term and source term are linearized by using values from the previous outer iterations. This kind of linearization requires many more iterations than a coupled technique such as Newton-like linearization. The number of outer iterations, however, can be substantially reduced by using multigrid techniques.

2 Mathematical Model

Flows in circular pipes are three-dimensional with respect to Cartesian coordinates, but they are two dimensional in cylindrical coordinates due to the symmetry over axis. In cylindrical coordinates, all derivatives with respect to the circumferential direction are zero and the three velocity components are functions of only the axial and radial directions. It is further assumed that there is no rotational flow around an axis, the circumferential velocity component disappears, and the governing equations can be further simplified. The 2D time-dependent equations for mass, momentum, and protein transport in conservative form for incompressible flow can be written as:

$$\frac{\partial \rho}{\partial t} + \frac{1}{r}\frac{\partial (r\rho v_r)}{\partial r} + \frac{\partial (\rho v_z)}{\partial z} = 0, \tag{3}$$

$$\frac{\partial (\rho v_r)}{\partial t} + \frac{1}{r}\frac{\partial (r\rho v_r v_r)}{\partial r} - \frac{1}{r}\frac{\partial}{\partial r}\left(r\mu\frac{\partial v_r}{\partial r}\right) + \frac{\partial (\rho v_r v_z)}{\partial z} - \frac{\partial}{\partial z}\left(\mu\frac{\partial v_r}{\partial z}\right) = -\frac{\partial p}{\partial r} - \mu\frac{v_r}{r^2}, \tag{4}$$

$$\frac{\partial (\rho v_z)}{\partial t} + \frac{1}{r}\frac{\partial (r\rho v_r v_z)}{\partial r} - \frac{1}{r}\frac{\partial}{\partial r}\left(r\mu\frac{\partial v_z}{\partial r}\right) + \frac{\partial (\rho v_z v_z)}{\partial z} - \frac{\partial}{\partial z}\left(\mu\frac{\partial v_z}{\partial z}\right) = -\frac{\partial p}{\partial z}, \tag{5}$$

$$\frac{\partial \phi}{\partial t} + \frac{1}{r}\frac{\partial (r v_r \phi)}{\partial r} + \frac{\partial (v_z \phi)}{\partial z)} = \frac{1}{r}\frac{\partial}{\partial r}\left(r\Gamma\frac{\partial \phi}{\partial r}\right) + \frac{\partial}{\partial z}\left(\Gamma\frac{\partial \phi}{\partial z}\right) + S, \tag{6}$$

where ρ is the density, μ the dynamic viscosity, p the dynamic pressure, and v_r and v_z are velocity components in the radial and axial directions, respectively, ϕ the concentration of protein, and S the source term. In the above equation set, independent variables are time t, radial coordinate r, and axial coordinate z.

3 Colocated Finite Volume Discretization

Cell-centered finite volume approach is applied to discretize the partial differential equations. The advantage of cell-centered arrangement is that second order accuracy is achieved, since the nodal value represents the mean over the control volume and the node is located at the centroid to the control volume.

Equations (3) $\sim$ (6) can be expressed in the form of convection-diffusion equation. Two-dimensional convection-diffusion equation in cylindrical axisymmetric coordinates may be written as

$$\frac{\partial}{\partial t}(\rho\phi) + \frac{1}{y}\frac{\partial}{\partial y}\left(y\rho v\phi - y\Gamma\frac{\partial\phi}{\partial y}\right) + \frac{\partial}{\partial x}\left(\rho u\phi - \Gamma\frac{\partial\phi}{\partial x}\right) = S. \tag{7}$$

In this expression, x and y are axial and radial coordinates, u and v are the velocity components in axial and radial directions, respectively. The reason to write an equation in axisymmetric coordinates in such a way is to facilitate programming, i.e., to let the same computer program perform calculations in both 2D Cartesian coordinates and axisymmetric ones. For the momentum equation in radial direction, an extra term of $-\frac{\Gamma v}{y^2}$ should be added to the right hand side of Eq. (7). It is worth noticing that the mass conservation equation is a special case of Eq. (7) in which ϕ, Γ, and S are taken as $\phi = 1$, $\Gamma = 0$, and $S = 0$. Integrating Eq. (7), the corresponding finite volume equations can be derived. For the mass conservation equation, the finite volume counterpart reads,

$$\frac{\rho_P - \rho_P^0}{\Delta t} + (F_e - F_w) + (F_n - F_s) = 0. \tag{8}$$

where $F_{e,w,n,s}$ each represents the mass flux at each of the four interfaces of the control volume. The finite volume expression of the momentum transport equations are written as

$$\frac{(\rho\phi)_P - (\rho\phi)_P^0}{\Delta t} + (J_e - J_w) + (J_n - J_s) = S_C + \phi_P S_P + S_{sym}. \tag{9}$$

where $J_{e,w,n,s}$ is the convection-diffusion flux at each of the four interfaces of the control volume, with $J_{e,w} = (\rho u\phi - \Gamma\frac{\partial\phi}{\partial x})_{e,w}$, $J_{n,s} = (\rho v\phi - \Gamma\frac{\partial\phi}{\partial y})_{n,s}$, S_C and S_P are the results of source term linearization, and S_{sym} is the contribution from axisymmetric coordinates, with $S_{sym} = -\Gamma\frac{v}{y^2}$ for the momentum equation of v. The approximation of convective flux is critical for an accurate solution. Frequently used methods include first order upwind and second order central difference. Here, a so-called "deferred correction" technique is employed for high-order flux approximation [3]. This technique calculate higher-order flux explicitly using values from the previous iteration.

The convection-diffusion terms in Eq. (9) are approximated in the following way, $J_{e,w,n,s} = A_{E,W,N,S}(\phi_P - \phi_{E,W,N,S})$. The finite volume representation of the 2D convection-diffusion equation can now be written as

$$\phi_P A_P + \phi_E A_E + \phi_W A_W + \phi_N A_N + \phi_S A_S = b, \tag{10}$$

where A_P, A_E, A_W, A_N, and A_S are coefficients, b is the source term. Their detailed expressions can be found in [6, 3].

The naive way of colocated arrangement makes the solution of Navier-Stokes equations not very pleasant due to the checkerboard pressure distribution. Therefore staggered grid was once

considered as a standard way for the calculation of incompressible flow [5, 6]. A remedy was proposed by van der Wijngaart [9] to deal with the pressure-velocity coupling on colocated grids by eliminating the oscillations in the pressure field. However this would introduce an inconsistency in pressure gradient [3]. This work uses colocated grid and adopts the remedy to filter out the oscillations due to the fact that colocated arrangement is attractive for non-orthogonal grid, complex geometry, and multigrid method.

4 Multigrid Methods

The initial guess in an iterative method is usually far from the converged solution, very frequently, a zero initial guess is used. It therefore makes sense to solve the equation first on a very coarse grid and use that solution to provide a better guess for the initial guess on the next finer grid. By the time we reach the finest grid, we already have a fairly good starting solution. Some iterative methods produce errors that are smooth functions of the spatial coordinates. In such methods, after a few iterations, the rapidly changing components of the error have been removed and the error becomes a smooth function of the spatial coordinates. If the error is smooth, the update can be computed on a coarser grid. Furthermore, iterative methods converge much faster on coarser grids. This suggests that much of the work can be done on a coarser grid. To do this the relationship between a fine grid and a coarse one has to be determined, which can be done by finite difference operators called restriction and prolongation. Restriction is to smooth the residual from the fine grid to the coarse one. Prolongation is to interpolate the updates or corrections from the coarse grid to the fine one.

The solution of Navier-Stokes equations consists of two loops, the inner iteration handles each of the individual equations of momentum, energy, and turbulent kinetics if necessary, and the outer iteration deals with the coupling and nonlinearity. For unsteady flow using implicit discretization, the linear equations need not be solved very accurately at each outer iteration. Usually a few iterations of a linear solver is enough. More accurate solution will not reduce the number of outer iterations but may increase the computing time. For steady flow calculation, the computation cost can be greatly saved by using a multigrid method.

In finite volume method on a structured grid, the multigrid version in 2D can be constructed such that each coarse grid control volume is composed of four control volumes of the next finer grid [3]. To do this, a grid generator that is able to generate multigrid is used. The grid generator takes input of the number of grid levels, the number of lines along each boundary, the coordinates of starting and ending points for each line, the line type, etc., for the coarsest grid. The data of the remaining levels of grids are computed automatically by subdividing each control volume in finer ones and saved as binary files to be loaded by the flow solver.

In the current work, a full multigrid procedure is used [7]. It starts on the coarsest grid until a converged solution is obtained. This solution is interpolated to the next finer grid to obtain a starting solution. After performing a few outer iterations on the finer grid, the calculation is moved to the coarser grid.

The algebraic equation Eq. (10) can be written as

$$A\phi = b, \tag{11}$$

where A is a square matrix, ϕ the unknown vector, b the source vector. After kth outer iterations on a grid with spacing h, the intermediate solution satisfies the following equation,

$$A_h^k \phi_h^k - b^k = r_h^k, \tag{12}$$

where r_h^k is the residual vector after the k iteration. Once the solution at the kth iteration is obtained, we restrict the solution as well as the residual to the the next coarse grid by the restriction operators I_h^{2h} and $\hat{I}_h^{2h}$. An approximate solution to the coarse grid problem can be found by solving the following system of equations,

$$A_{2h}\phi_{2h}^1 = A_{2h}(I_h^{2h}\phi_h^k) - \hat{I}_h^{2h} r_h^k. \tag{13}$$

After the solution on the coarse grid is obtained, the correction $\Delta\phi = \phi_{2h}^1 - \phi_{2h}^0$ is transfered to the fine grid by interpolation, where $\phi_{2h}^0 = I_h^{2h}\phi_h^k$. The difference of I_h^{2h} and $\hat{I}_h^{2h}$ is as follows, I_h^{2h} takes the mean value of states in a set of cells, but $\hat{I}_h^{2h}$ performs a summation of residuals over a set of cells. The value of ϕ_h^k is updated by

$$\phi_h^{k+1} = \phi_h^k + I_{2h}^h \Delta\phi, \tag{14}$$

where I_{2h}^h is a prolongation operator. This procedure is repeated until the solution on the finest grid converges using multigrid V-cycle [7]. The smoother in the multigrid method is Stone's strong implicit procedure (SIP), which is a modification from the standard ILU decomposition [8]. This paper has adapted the multigrid method for incompressible Navier-Stokes equations provided by Schreck [7] and extended it to include mass transport. Since the concentration of ligand is very small, in the order of 10^{-11} to 10^{-10} mol, we may assume that the momentum and mass transfer equations are independent of each other. Consequently the momentum transfer equation can be solved first to obtain the velocity distribution, which is then put into the mass transfer equation. The modified multigrid algorithm for incompressible flow and mass transfer is presented as Algorithm 1.

5 Numerical Example

The dimensions of the capillary under consideration are length $L = 0.1$ m and radius $R = 0.00035$ m. The ratio of length over diameter is 286. To simulate capillary flow, four types of boundary conditions are used in the numerical simulation: inlet boundary to the left-hand side, outlet boundary to the right-hand side, symmetry boundary at the bottom, and impermeable wall boundary at the top. For inlet boundary, all quantities are prescribed, and the incoming convective flux is calculated as well. For outlet boundary, zero gradient along grid line is applied. A three-level multigrid is considered, as shown in Fig. 1, and the number of control volumes are 40×5, 80×10, and 160×20, respectively. First the coarsest grid is initialized, and each time the grid is refined, one control volume is divided into four smaller control volumes.

Algorithm 1 Multigrid Algorithm for Incompressible Flow and Mass Transfer

while $levelOfGrid < levelOfGrid_{max}$ **do**
  Extrapolate from coarse to fine grid, $(u, v, p, \phi)^{levelOfGrid} \leftarrow (u, v, p, \phi)^{levelOfGrid-1}$
  while $t < t_{stop}$ **do**
    Save data at time $t-2$, $(u, v, \phi)^{t-2} \leftarrow (u, v, \phi)^{t-1}$
    Save data at time $t-1$, $(u, v, \phi)^{t-1} \leftarrow (u, v, \phi)^{t}$
    while $outerIter < outIter_{max}$ **do**
      solve for u
      solve for v
      solve for p
      $residual = \text{Max}(residual_u, residual_v, residual_p)$
      if $residual > largeNumber$ **then**
        exit "Diverge"
      else if $residual > convergenceCritiaria$ **then**
        for $i = levelOfGrid$; $i > 1$; $i--$ **do**
          Restriction
        end for
        for $i = 1$;$i < levelOfGrid$;$i++$ **do**
          Prolongation
        end for
      else
        Break
      end if
    end while
    solve for ϕ
  end while
end while

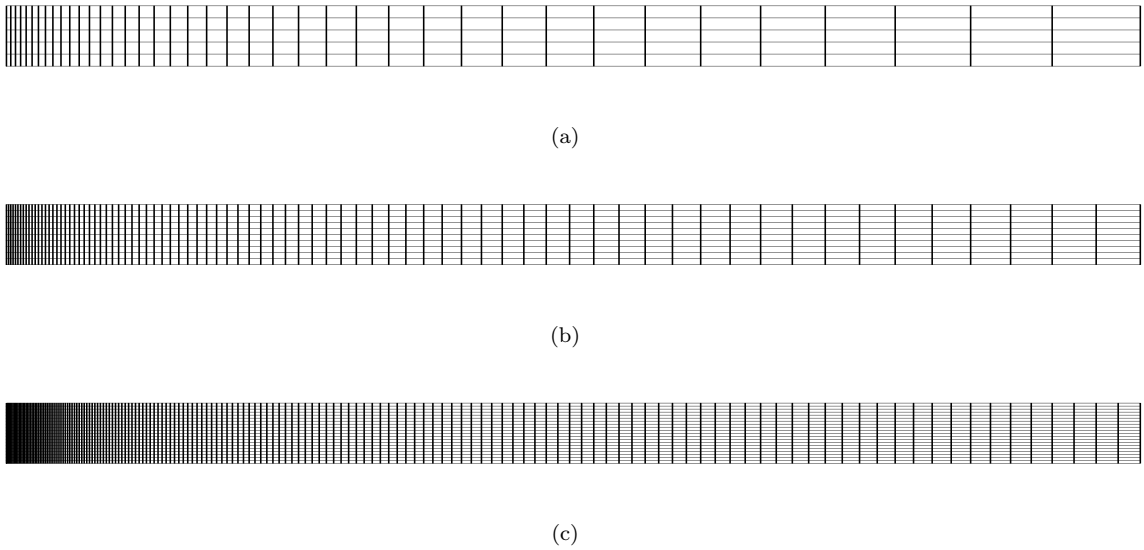

(a)

(b)

(c)

Figure 1: Numerical grids for capillary flow and protein transport. (a) First level grid. (b) Second level grid. (c) Third level grid.

Table 1: The rate of concentration change due to protein interactions.

Reaction rate	Parameters
$\frac{d[R]}{dt} = -k_f^R[L][R] + k_r^R[C] + k_r^T[T] - k_c[R][G]$ $-k_{int}[R] + V_R$	$k_f^R = 2.5 \times 10^8 \mathrm{M}^{-1}\mathrm{min}^{-1}$ $k_r^R = 0.048\mathrm{min}^{-1}$, $k_r^T = 0.001\mathrm{min}^{-1}$ $k_c = 0.001\mathrm{min}^{-1}$, $k_{int} = 0.005\mathrm{min}^{-1}$
$\frac{d[P]}{dt} = -k_f^P[L][P] + k_r^P[G] + k_r^T[T] - k_c[C][P]$ $-k_{int}[P] + V_P$	$k_f^P = 0.9 \times 10^8 \mathrm{M}^{-1}\mathrm{min}^{-1}$ $k_r^P = 0.068\mathrm{min}^{-1}$, $k_r^T = 0.001\mathrm{min}^{-1}$ $k_c = 0.001\mathrm{min}^{-1}$, $k_{int} = 0.005\mathrm{min}^{-1}$
$V\frac{d[L]}{dt} = -k_f^R[L][R] + k_r^R[C] + k_r^T[T] - k_f^P[L][P]$ $-k_r^R[G]$	$k_f^R = 2.5 \times 10^8 \mathrm{M}^{-1}\mathrm{min}^{-1}$ $k_f^P = 0.9 \times 10^8 \mathrm{M}^{-1}\mathrm{min}^{-1}$ $k_r^R = 0.048\mathrm{min}^{-1}$, $k_r^T = 0.001\mathrm{min}^{-1}$
$\frac{d[C]}{dt} = k_f^R[L][R] - k_r^R[C] - k_c[C][P] - k_c[C]^2$ $+2k_{uc}[C_2] - k_{int}[C]$	$k_f^R = 2.5 \times 10^8 \mathrm{M}^{-1}\mathrm{min}^{-1}$ $k_r^R = 0.048\mathrm{min}^{-1}$, $k_c = 0.001\mathrm{min}^{-1}$ $k_{uc} = 1\mathrm{min}^{-1}$, $k_{int} = 0.005\mathrm{min}^{-1}$
$\frac{d[C_2]}{dt} = \frac{k_c}{2}[C]^2 - k_{uc}[C_2] - k_{int}^D[C_2]$	$k_c = 0.001\mathrm{mint}^{-1}$, $k_{uc} = 1min^{-1}$ $k_{int}^D = 0.078\mathrm{min}^{-1}$
$\frac{d[G]}{dt} = -k_f^R[L][R] + k_r^R[C] + k_r^T[T] - k_c[R][G]$ $-k_{int}[R]$	$k_f^R = 2.5 \times 10^8 \mathrm{M}^{-1}\mathrm{min}^{-1}$ $k_r^R = 0.048\mathrm{min}^{-1}$, $k_r^T = 0.001\mathrm{min}^{-1}$ $k_c = 0.001\mathrm{min}^{-1}$, $k_{int} = 0.005\mathrm{min}^{-1}$
$\frac{d[G_2]}{dt} = \frac{k_c}{2}[G]^2 - k_{uc}[G_2] - k_{int}[G_2]$	$k_c = 0.001\mathrm{min}^{-1}$, $k_{uc} = 1\mathrm{min}^{-1}$ $k_{int}^D = 0.078\mathrm{min}^{-1}$
$\frac{d[T]}{dt} = k_c[R][G] + k_c[C][P] - k_r^T[T] - k_c[T]^2$ $+2k_{uc}[T_2] - k_{int}[T]$	$k_c = 0.001\mathrm{min}^{-1}$, $k_r^T = 0.001\mathrm{min}^{-1}$ $k_{uc} = 1\mathrm{min}^{-1}$, $k_{int} = 0.005\mathrm{min}^{-1}$
$\frac{d[T_2]}{dt} = \frac{k_c}{2}[T]^2 - k_{uc}[T_2] - k_{int}^D[T_2]$	$k_c = 0.001\mathrm{min}^{-1}$, $k_{uc} = 1min^{-1}$ $k_{int}^D = 0.078\mathrm{min}^{-1}$

The protein interactions in capillary are modeled as the transport of ligand in the flow and ligand-receptor binding and signaling on the capillary surface. This is actually a problem of mass transfer with reactive boundary conditions. For the mass transport equation, the boundary conditions are: given concentration on the west, zero flux on the east, symmetrical condition on the south, and reaction boundary on the north. An existing model of biochemical reactions on the capillary surface from Forsten-Williams [4] and Fannon [2] has been used in our simulation. The biochemistry model is shown in Table 1, where the reaction rates of all involved proteins are represented by a series of ordinary differential equations (ODEs), and the parameters in the equations are determined by experimental measurement or theoretical estimation. Details of the model can be found in works of Forsten-Williams [4] and Fannon [2]. The system of ordinary differential equations are solved by a variable-coefficient ODE solver VODE for stiff and nonstiff systems of initial value problems [1].

The code is developed for transient flow, and the steady-state solution is presented, where a very large time step $\Delta t = 1.0E20$ s is chosen. The computation is performed on a Sun-Blade-100 machine with a single 500 MHz SPARC processor and 2 GB memory. The numerical results of ligand field is plotted in Fig.2, where the ligand concentration is non-dimensionalized with respect to the inlet concentration on the west boundary. It clearly shows that the concentration of ligand in the capillary is spatially reduced down the capillary due to biochemical reactions on the surface.

Figure 3(a) displays the convergence history for capillary flow in a single grid with finest grid

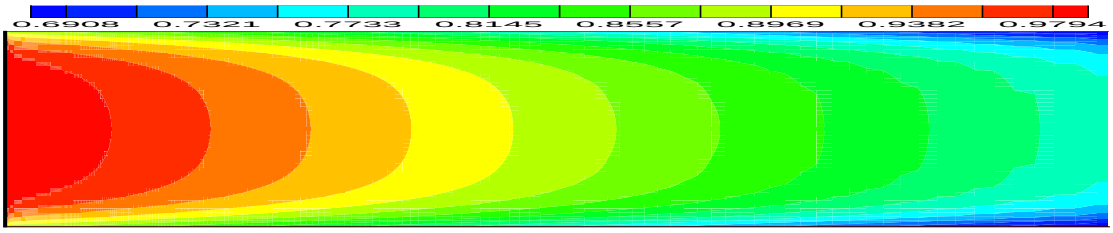

Figure 2: Steady state solution of ligand field in a capillary

Table 2: Performance Comparison of multigrid method with different linear solvers

Solver	Mesh	No. Outer Iterations		CPU-Time (s)		Speed-up Ratio
		Single-grid	Multigrid	Single-grid	Multigrid	
SIP	40×5	234	234	0.41	0.41	1.0
	80×10	898	28	6.87	0.64	10.7
	160×20	6000	54	176.45	5.39	32.7
BiCGSTAB	40×5	114	114	0.35	0.35	1.0
	80×10	432	26	5.24	0.56	9.36
	160×20	6000	50	174.66	5.43	32.16
GMRES	40×5	101	101	0.22	0.22	1.0
	80×10	389	23	5.43	0.55	9.87
	160×20	6000	52	186.75	5.82	32.08

spacing. In current calculation, the energy equation is not considered. The results clearly show that the residuals are reduced effectively in the first 200 outer iterations, and after that, they can not be further eliminated no matter how many more outer iterations are performed. In capillary flow (Fig. 3(a)), the pressure equation has a relatively large residual.

The performances between single-grid and multigrid are compared in Fig. 3(b), where the number of iterations means the number of outer iterations in the finest grid. As it has been shown that a large residual is from the pressure equation in flow simulation, here only the comparison of pressure residual is presented, see Fig. 3. In single-grid, the pressure residual can only be reduced to the order of 10^{-3}, while in the case of three-level multigrid, it can be reduced to the order of 10^{-5} within less than 100 outer iterations. Table 2 lists the number of outer iterations, CPU-time, and speed-up ratio for capillary flow with various mesh size and different linear solvers. In Table 2, the recorded CPU-time for multigrid is the total computing time for all levels of grids that are involved. The speed-up ratio for capillary flow can be over 30 and 20 respectively in the finest grid. It can be concluded that multigrid technique can reduce computation time significantly for both capillary flow and protein transport. Three iterative solvers, SIP, BiCGSTAB and GMRES have been used to solve the inner linear system and their performance are compared. In this particular case, the linear systems are five diagonal matrixes due to finite volume discretization of two-dimensional partial differential equations in axisymmetrical coordinates, BiCGSTAB and GMRES solvers do not have obvious advantages over SIP in reducing the number of outer iterations of Navier-Stokes equations in multigrid.

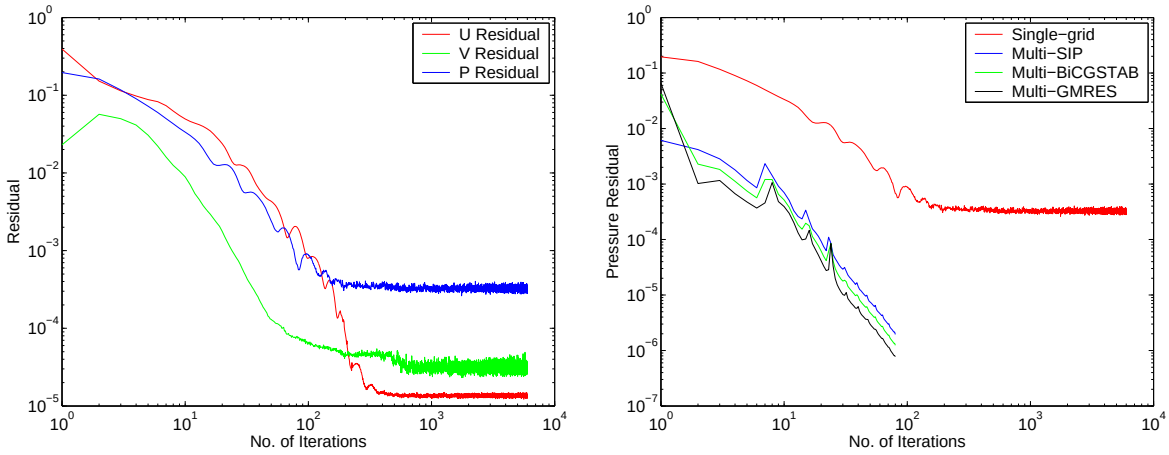

(a) (b)

Figure 3: Comparison of convergence history between single-grid and multigrid. (a) Residuals of pressure and velocities in single grid. (b) Comparison of pressure residuals between single-grid and multigrid with different linear solvers

6 Conclusion

This paper presents the numerical solution of ligand transport and protein interactions in a capillary. The capillary flow is predicted using incompressible Navier-Stokes equations by the finite volume method with colocated mesh arrangement with the assumption that the capillary is a circular pipe. To reduce the computation cost, a multigrid V-cycle technique is applied for the nonlinear Navier-Stokes equations, which includes restriction and prolongation to restrict fine grid solution to coarse grid, and to interpolate coarse grid solution to fine grid. The multigrid method is extended to solve mass transfer equation. Results indicate that the multigrid method can save CPU time substantially. The computed profile of ligand distribution in the capillary is presented.

References

[1] P. N. Brown, G. D. Byrne, and A. C. Hindmarsh, VODE: A variable coefficient ODE solver, *SIAM J. Sci. Stat. Comput.*, **10**, pp. 1038-1051, 1989.

[2] M. Fannon, K. Forsten-Williams, C. J. Dowd, D. A. Freedman, J. Folkman, and M. A. Nugent, Binding inhibition of angiogenic factors by heparan sulfate proteoglycans in aqueous humor: potential mechanism for maintenance of an avascular environment. *The FASEB Journal*, **17**, pp. 902-904, 2003.

[3] J. H. Ferziger and M. Perić, *Computational Methods for Fluid Dynamics*, Springer, Berlin, 1999.

[4] K. Forsten-Williams, C. C. Chua, and M. A. Nugent, The kinetics of FGF-2 binding to heparan sulfate proteoglycans and MAP kinase signaling. *Journal of Theoretical Biology*, **233**, pp. 483-499, 2005.

[5] F. H. Harlow and J. E. Welsh, Numerical calculation of time dependent viscous incompressible flow with free surface, *Physics and Fluids*, **8**, 2182-2189, 1965.

[6] S. V. Patankar, *Numerical Heat Transfer and FluidFlow*, The McGraw-Hill Company, Inc., New York, 1980.

[7] E. Schreck and M. Perić, Computation of fluid flow with a parallel multigrid solver. *International Journal for Numerical Methods in Fluids*, **16**, 303-327, 1993.

[8] H. L. Stone, Iterative solution of implicit approximations of multidimensional partial differential equations, *SIAM Journal of Numerical Analysis*, **5**, 530-558, 1968.

[9] R. J. F. van der Wijngaart, Composite grid techniques and adaptive mesh refinement in computational fluid dynamics, Report CLaSSiC-90-07, Department of Computer Science, Stanford University, 1990.